AGU PUBLICATIONS

Geophysical Research Letters

RESEARCH LETTER
10.1002/2016GL071026

Key Points:
- Change point detection allows precise characterization of monsoon seasonal evolution and timescales
- Transition between negative and positive net precipitation at onset and retreat
- Index provides insight into relationship between local and large-scale monsoon timing

Supporting Information:
- Supporting Information S1

Correspondence to:
J. M. Walker,
jwalker@caltech.edu

Citation:
Walker, J. M. and S. Bordoni (2016), Onset and withdrawal of the large-scale South Asian monsoon: A dynamical definition using change point detection, *Geophys. Res. Lett.*, *43*, 11,815–11,822, doi:10.1002/2016GL071026.

Received 2 SEP 2016
Accepted 4 NOV 2016
Accepted article online 14 NOV 2016
Published online 22 NOV 2016

©2016. American Geophysical Union. All Rights Reserved.

Onset and withdrawal of the large-scale South Asian monsoon: A dynamical definition using change point detection

Jennifer M. Walker[1] and Simona Bordoni[1]

[1] Environmental Science and Engineering, California Institute of Technology, Pasadena, California, USA

Abstract We introduce an objective definition for onset and withdrawal of the South Asian summer monsoon (SASM), based on the large-scale atmospheric moisture budget. The change point (CHP) index allows precise characterization of the different stages and timescales of the large-scale SASM and is highly correlated with the local operational index, the monsoon onset over Kerala. The CHP-based onset and withdrawal dates, which capture the expected seasonal transitions in rainfall and winds, correspond with regime changes in the SASM moisture budget between negative and positive net precipitation. Climatological composites reveal that the seasonal transitions in SASM sector mean precipitation and circulation closely resemble those of the zonal mean Hadley circulation. The CHP index at grid points within the SASM domain yields a robust definition of local onset and withdrawal dates, which are well correlated with the large-scale index on interannual timescales, providing insight into the regional variability of the SASM.

1. Introduction

The onset of the South Asian summer monsoon (SASM) is marked by a sharp increase in rainfall and abrupt reversal of winds over South Asia. Accurately defining and forecasting this transition is critical for effective agriculture planning and water management in the region [e.g., *Raju et al.*, 2007; *Adamson and Nash*, 2012]. Many different measures of SASM onset exist, but there is no widely accepted objective definition. The India Meteorological Department (IMD) employs the monsoon onset over Kerala (MOK) as an operational index, using a subjective method based on rain gauge data, winds, and outgoing longwave radiation [*Rao*, 1976; *Ananthakrishnan and Soman*, 1988]. Objective definitions of SASM onset include measures such as the increase of rainfall above a threshold [*Wang and LinHo*, 2002], transitions in vertically integrated moisture transport [*Fasullo and Webster*, 2003], reversal of surface wind [*Ramage*, 1971], and intensification of the lower level Somali jet [*Taniguchi and Koike*, 2006; *Wang et al.*, 2009].

Having been developed for specific applications, such as operational forecasts and evaluation of observed variability, existing definitions are generally not well suited for broader use. The MOK cannot be extended to identify SASM onset in climate model simulations, due to its subjective methodology. Objective indices are mostly threshold based, and sensitivity to the selected threshold can yield onset dates that vary significantly with slightly different thresholds; this issue is especially critical when comparing data sets or climate models, which may have different biases in their mean climatologies. Threshold-based indices are also susceptible to false onsets due to premonsoon rainfall peaks and wind anomalies caused by transient weather systems [e.g., *Fieux and Stommel*, 1977; *Flatau et al.*, 2001; *Noska and Misra*, 2016].

In this study, we introduce an objective definition of large-scale SASM onset and withdrawal which does not require selection of any threshold. This index is based on change point detection of the atmospheric moisture flux converging in the large-scale SASM sector (see section 3) and robustly represents the seasonal transitions in SASM circulation and precipitation.

2. Data

Atmospheric fields for the years 1980–2015 are used from NASA's Modern-Era Retrospective analysis for Research and Applications, Version 2 (MERRA-2) [*Rienecker et al.*, 2011; *Bosilovich et al.*, 2015]. We use pressure-level winds and vertically integrated moisture fluxes, at a horizontal grid resolution of 0.5° (latitude) × 0.625° (longitude). Daily means are computed from the 3-hourly reanalysis. For precipitation, we use daily

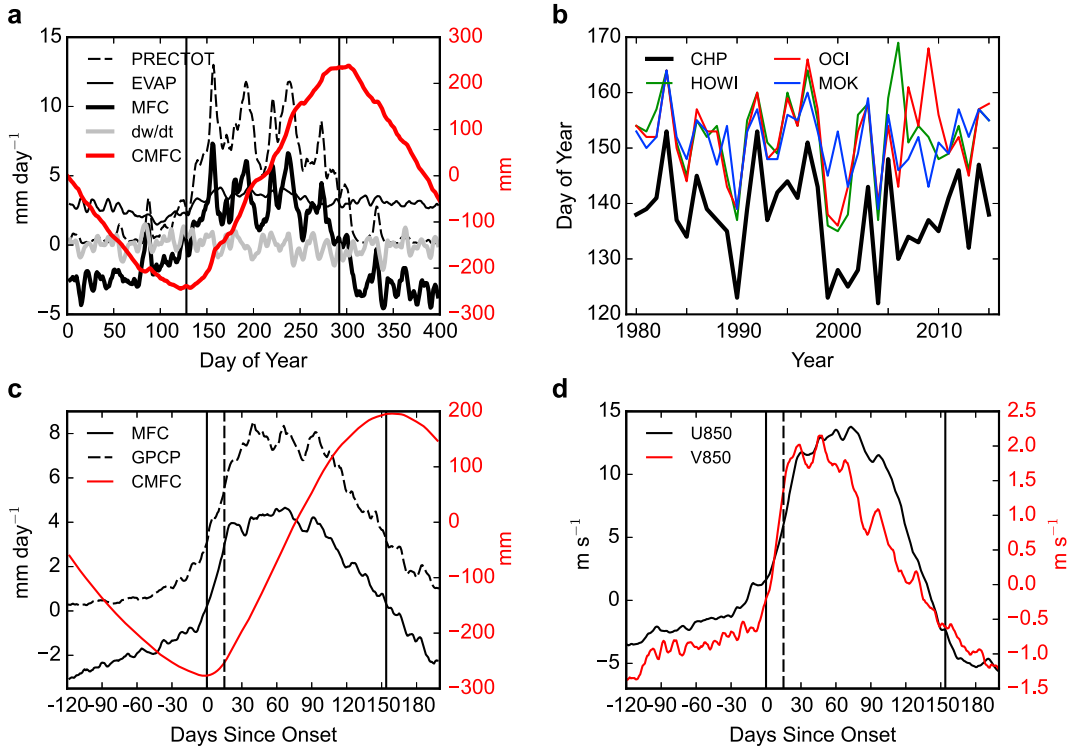

Figure 1. (a) Example time series of MERRA-2 daily atmospheric moisture budget averaged over 10–30°N, 60–100°E in the year 2000 (1 January 2000 to 3 February 2001), showing the total precipitation (dashed black), evaporation (solid black), MFC (heavy solid black), atmospheric storage (solid gray), and CMFC (red). Vertical black lines indicate the onset and withdrawal days in this year. (b) Yearly onset dates defined by CHP (heavy black), HOWI (green), OCI (red), and MOK (blue). (c, d) Climatological composites of MERRA-2 (1980–2015) and GPCP (1997–2015) daily fields centered on onset date, averaged 60–100°E, with vertical black lines indicating mean onset and withdrawal days and dashed vertical black line indicating the start of the mature stage (day 15). Moisture budget averaged 10–30°N, showing MFC (solid black, mm d^{-1}), GPCP (dashed black, mm d^{-1}), and CMFC (red, mm) (Figure 1c). 850 hPa zonal (black) and meridional (red) winds at 15°N (m s^{-1}) (Figure 1d).

estimates at 1° × 1° grid resolution from the Global Precipitation Climatology Project (GPCP) Version 1.2 One-Degree Daily [*Huffman et al.*, 2001; *Huffman et al.*, 2016] from 1997 (first complete year available) to October 2015 (final month available).

Statistical significance of correlation coefficients are computed with a Student's *t* test, and correlations which are statistically significant at the 5% level are highlighted.

3. SASM Onset and Withdrawal Index

3.1. Index Definition

Following the approach of our previous work on the interannual variability of the SASM [*Walker et al.*, 2015], we define the SASM region as 10–30°N, 60–100°E (Figure S1, further details in the supporting information) and we analyze seasonal transitions in its large-scale atmospheric moisture budget, given by

$$\mathrm{MFC} = -\int_0^{p_s} \nabla_p \cdot (\mathbf{u}\, q)\frac{\mathrm{d}p}{g} = P - E + \frac{\partial w}{\partial t} \tag{1}$$

where MFC is the horizontal moisture flux convergence integrated from the surface to the top of the atmosphere, $\nabla_p \cdot ()$ the horizontal divergence in pressure coordinates, $\mathbf{u} = (u, v)$ the horizontal wind vector, q the specific humidity, P the precipitation rate, E the evaporation rate, and $w = \int_0^{p_s} q\frac{\mathrm{d}p}{g}$ the total precipitable water. With negligible storage $\partial w/\partial t$ (e.g., Figure 1a), the dominant balance in the SASM region is between MFC and net precipitation (*P*-*E*). Thus, positive (negative) values of MFC correspond to positive (negative) net precipitation.

Table 1. Summary of CHP Indices of Large-Scale SASM Onset, Withdrawal, and Season Length

	Mean	Standard Deviation	Maximum	Minimum
Onset date	138 (18 May)	8	153 (2 Jun)	122 (2 May)
Withdrawal date	292 (19 Oct)	9	311 (7 Nov)	273 (30 Sep)
Season length	154	13	186	130

We define a change point (CHP) index for SASM onset and withdrawal, adapted from the method of *Cook and Buckley* [2009] as follows: In each year, we compute the MERRA-2 daily mean MFC, averaged over the SASM region. We then construct a cumulative time series of MFC accumulated since 1 January of each year (CMFC). We use a two-phase linear regression of CMFC versus day of year to detect change points over two ranges: days 1–250 for monsoon onset and days 200–400 for monsoon withdrawal, where the days above 365 (366 in leap years) are from the beginning of the following year.

Figure 1a shows an example of the moisture budget terms from equation (1), the CMFC time series, and CHP onset and withdrawal, for the year 2000. The onset captures the first burst of monsoonal rainfall, followed by active-break rainfall cycles throughout the season. The CHP onset (withdrawal) day corresponds approximately to the minimum (maximum) of the CMFC time series and to the transition from negative to positive values (positive to negative) of daily MFC, a consistent feature in all years. Thus, our definition of onset corresponds with a moisture budget transition from negative to positive net precipitation (and vice versa for withdrawal).

Figure 1b shows the CHP onset dates in each year, while Table 1 and Figure S2a provide summary statistics of the onset, withdrawal, and season lengths, defined as the number of days from onset to withdrawal. The climatological mean onset is day 138 (18 May), withdrawal is day 292 (19 October), and season length is 154 days, with standard deviations of 8, 9, and 13 days, respectively. In the supporting information, we discuss interannual variability in SASM timing associated with El Niño–Southern Oscillation [*Goswami*, 2005; *Huang et al.*, 2015]. We also show that earlier onsets are associated with longer seasons and hence enhanced seasonal rainfall (Figure S8 and Table S1).

3.2. Index Performance and Comparison With Other Definitions

To assess representativeness of the CHP index and investigate transitions in circulation and precipitation at SASM onset and withdrawal, we compute climatological composites of daily fields centered on the onset (withdrawal) date in each year, so that day 0 corresponds to onset (withdrawal) day. These composites are smoothed with a centered 5 day moving average. Figures 1c and 1d show composites, centered on onset date, of various precipitation and circulation indices averaged in longitude over the SASM sector (60–100°E). In Figure 1c, we see that the onset day marks the beginning of a sharp increase in rainfall over the SASM region. Note that the GPCP precipitation time series shown here is independent of the MERRA-2 moisture budget and CHP calculations. Figure 1d shows 850 hPa zonal (U850) and meridional (V850) winds at 15°N, representing the lower level flow across the Arabian Sea, Indian peninsula, and Bay of Bengal. Around day 0, there is an abrupt transition in both U850 and V850 from weak negative to strong positive values, indicating wind reversal and development of strong southwesterly flow.

Thus, the CHP index robustly characterizes the distinguishing features of SASM onset: initiation of heavy monsoon rain and reversal of lower level winds. The climatological composites centered on withdrawal date (Figure S2) show opposite but much more gradual transitions at withdrawal, in agreement with previous studies [*Webster and Yang*, 1992; *Fasullo and Webster*, 2003; *Cook and Buckley*, 2009].

For comparison with previously defined indices, we consider the MOK dates provided by the IMD and we use MERRA-2 to calculate two previously introduced dynamically based indices for the large-scale SASM: the hydrologic onset and withdrawal index (HOWI) [*Fasullo and Webster*, 2003], based on transitions in vertically integrated moisture fluxes averaged over the Arabian Sea, and the onset circulation index (OCI) [*Wang et al.*, 2009], based on a threshold in 850 hPa zonal wind averaged over the Southern Arabian Sea. Figure 1b shows the yearly onset dates defined by these indices. High correlations and lead-lag relationships between them are evident. For MOK, HOWI, and OCI, the climatological mean onset ranges from days 151 to 152 (31 May to 1 June), whereas the climatological mean CHP onset is 13–14 days earlier, on day 138 (18 May). This offset is due to CHP onset representing the beginning of the transition (i.e., the change point) rather than the first day

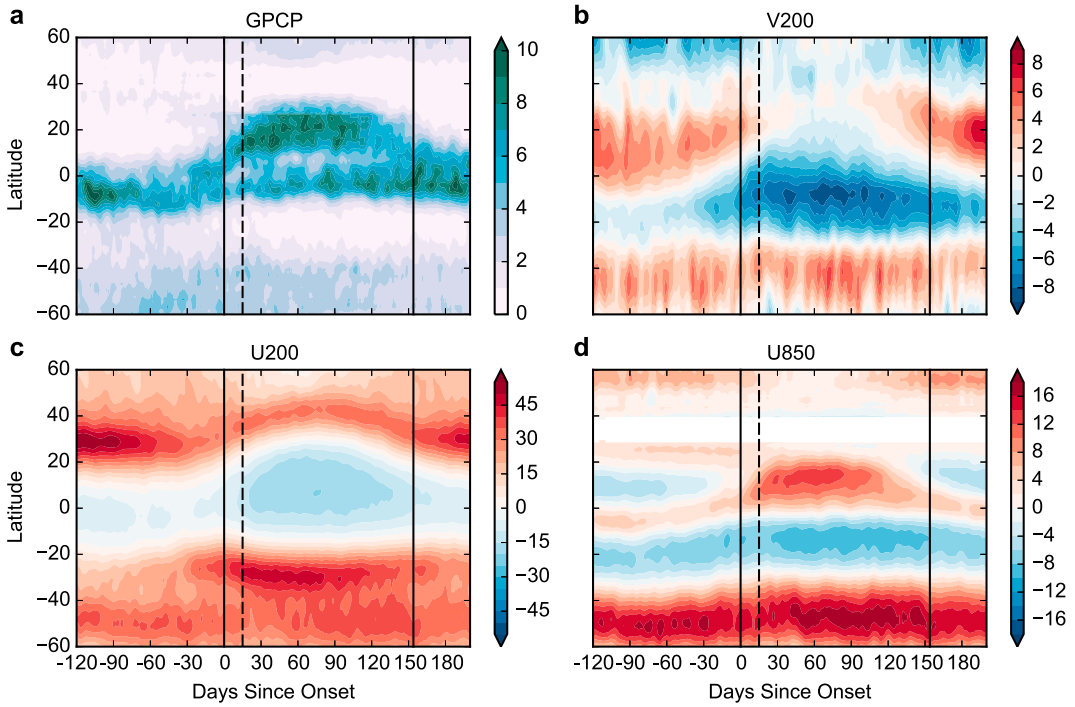

Figure 2. Seasonal evolution of (a) GPCP and (b–d) MERRA-2 climatological composites centered on onset date, averaged 60–100°E: precipitation (mm d^{-1}) (Figure 2a), 200 hPa meridional wind (m s^{-1}) (Figure 2b), 200 hPa zonal wind (m s^{-1}) (Figure 2c), and 850 hPa zonal wind (m s^{-1}) (Figure 2d). Vertical black lines indicate mean onset and withdrawal days, and dashed vertical black line indicates the start of the mature stage (day 15). Latitudes with less than 50% of grid points above the topography are masked out in Figure 2d.

when the monsoon rain and winds are well established, as represented by the other definitions. Interannual variability of CHP onset is highly correlated with the other indices, with correlation coefficients of 0.82, 0.73, and 0.76 with MOK, HOWI, and OCI, respectively. CHP is also more highly correlated with the operational MOK onset than the other two dynamically based indices, with correlation coefficients of 0.82, 0.62, and 0.56 of MOK with CHP, HOWI, and OCI, respectively.

There are numerous advantages to the CHP index in defining seasonal monsoon transitions. Since no thresholds are used, this method is not hindered by the pitfalls of threshold-based indices discussed in section 1. By construction, the CHP index is not susceptible to false onsets or withdrawals because change points are detected taking into account the MFC at all days in the given range, rather than considering only the values on a single day or few days. Finally, since change points represent the beginning of the onset or withdrawal transition, rather than a day somewhere in the midst of the transition, this definition allows us to characterize more precisely the duration of the transition and to construct composites elucidating the different timescales of the various stages of the monsoon, as discussed in the next section.

4. Seasonal Transitions

4.1. Large-Scale Circulation and Precipitation

Figure 2 shows the seasonal evolution of climatological composites, centered on onset date, of GPCP precipitation and MERRA-2 upper level (200 hPa) and lower level (850 hPa) winds, averaged over 60–100°E. In each field, we see a gradual seasonal transition over approximately 2 months preceding onset ("premonsoon" stage), followed by an abrupt transition from day 0 to approximately day 15 ("onset" stage). By day 15, mature monsoon conditions are well established, persisting for approximately three months ("mature" stage). The "withdrawal" stage is much more gradual than the onset stage, with a gradual retreat of monsoon rains and a transition in winds occurring slowly over approximately the final 1.5 months of the season (Figures S2b, S2c, and S3).

During the premonsoon stage, the SASM sector Intertropical Convergence Zone (ITCZ), indicated by the latitude of maximum precipitation, migrates across the equator from approximately 10°S to approximately 2°N

(Figure 2a). A corresponding transition is evident in the upper level meridional wind (V200). The V200 field represents the upper level flow of the large-scale meridional overturning circulation in the SASM sector, as previously shown in the Eulerian mass stream function for the seasonal mean monsoon [*Bordoni and Schneider*, 2008; *Walker et al.*, 2015]. During the premonsoon stage, there are a pair of regional Hadley cells, with the Northern Hemisphere (NH) cell initially stronger. As the Southern Hemisphere (SH) cell expands into the NH and the ITCZ migrates northward across the equator, the SH cell strengthens while the NH cell contracts and weakens (Figure 2b). Concurrent with the transition in precipitation and V200, the upper level westerly jet in the NH weakens and migrates northward, while a subtropical westerly jet starts to develop in the SH (Figure 2c).

Around day 0, as the SASM moisture budget transitions from negative to positive net precipitation, we observe a basin-wide switch of the lower level zonal winds over the Arabian Sea from negative to positive (Figure S4), so that the lower level NH tropical trade winds are reversed over the entire SASM sector (Figures S4 and 2d). The lower level southerly jet off the eastern coast of Africa (Somali jet) also begins to develop around day 0 over an extended longitudinal range (Figure S5). By the end of the onset stage (day 15), strong lower level southwesterly flow has developed across the SASM region, with maximum lower level westerly and southerly wind speeds exceeding 10 m s^{-1} (Figures S4 and S5).

During the onset stage, the ITCZ migrates rapidly northward to approximately 15°N as the SH Hadley cell suddenly intensifies and expands deep into the NH, while the NH Hadley cell almost disappears (Figures 2a and 2b). Accompanying this transition is an abrupt strengthening and expansion of upper level tropical easterlies, northward migration of the NH upper level westerly jet, and strengthening of the SH upper level subtropical jet (Figure 2c).

While consistent with previous findings for the SASM [e.g., *Webster and Yang*, 1992; *Li and Yanai*, 1996; *Trenberth et al.*, 2005], these sector mean seasonal transitions in precipitation and winds also bear close resemblance to seasonal transitions of the zonal mean Hadley circulation, which shifts from the traditional equinoctial pattern characterized by a pair of Hadley cells during equinox seasons to a solsticial pattern dominated by a single cross-equatorial winter cell and a very weak or negligible summer cell during summer seasons [*Dima and Wallace*, 2003; *Nguyen et al.*, 2013; *Shaw*, 2014]. These similarities suggest that the SASM projects strongly on the zonal mean Hadley cell during NH summer and can be understood, at least to some extent, in terms of recent theories of zonally symmetric, angular momentum-conserving overturning circulations [e.g., *Gadgil*, 2003; *Privé and Plumb*, 2007; *Bordoni and Schneider*, 2008].

The 15 day timescale of the SASM onset transition is very abrupt compared to the seasonal cycle of insolation, which is strongly dominated by annual and semiannual Fourier harmonics [*Weickmann and Chervin*, 1988; *Boos and Emanuel*, 2009]. From day 0 to day 15, GPCP precipitation over the SASM region almost doubles, from 3.1 mm d^{-1} to 5.6 mm d^{-1}, and near-surface flow across the SASM sector at 15°N transitions from weak westerly zonal wind (1.6 m s^{-1}) to strong westerly zonal wind (6.0 m s^{-1}) and from northerly meridional wind (−0.2 m s^{-1}) to southerly meridional wind (1.4 m s^{-1}) (Figures 1c and 1d). To reproduce the same 15 day transitions in these GPCP, U850, and V850 time series with a best fit of the first n Fourier harmonics (based on residual least squares minimization) requires at least $n = 8$, corresponding to much higher frequency variability than the seasonal cycle of insolation.

4.2. Spatial Characteristics and Local Onset

While our index represents transitions in the large-scale SASM rather than a single region of its domain, it is of interest to explore spatial patterns of rainfall progression at and after monsoon onset. These are shown in Figure 3 through climatological composites, centered on onset date, of GPCP precipitation on various days in the monsoon season. The rain belt propagation follows a similar progression as seen in previous studies [*Wang and LinHo*, 2002; *Wang et al.*, 2009]: Monsoon rainfall initially develops over the eastern equatorial Indian Ocean, eastern Bay of Bengal, Andaman Sea, Myanmar, and Thailand (days 0–5). By day 15, rains are established over Kerala, followed by a gradual northward progression into the Indian subcontinent over the following weeks.

To investigate the spatial characteristics of monsoon transitions over the SASM region, and the relation of local onset (withdrawal) dates with our large-scale index, we adapt the CHP method to define local onset (withdrawal) dates at each grid point. Rather than using CMFC, which can be very noisy at individual grid

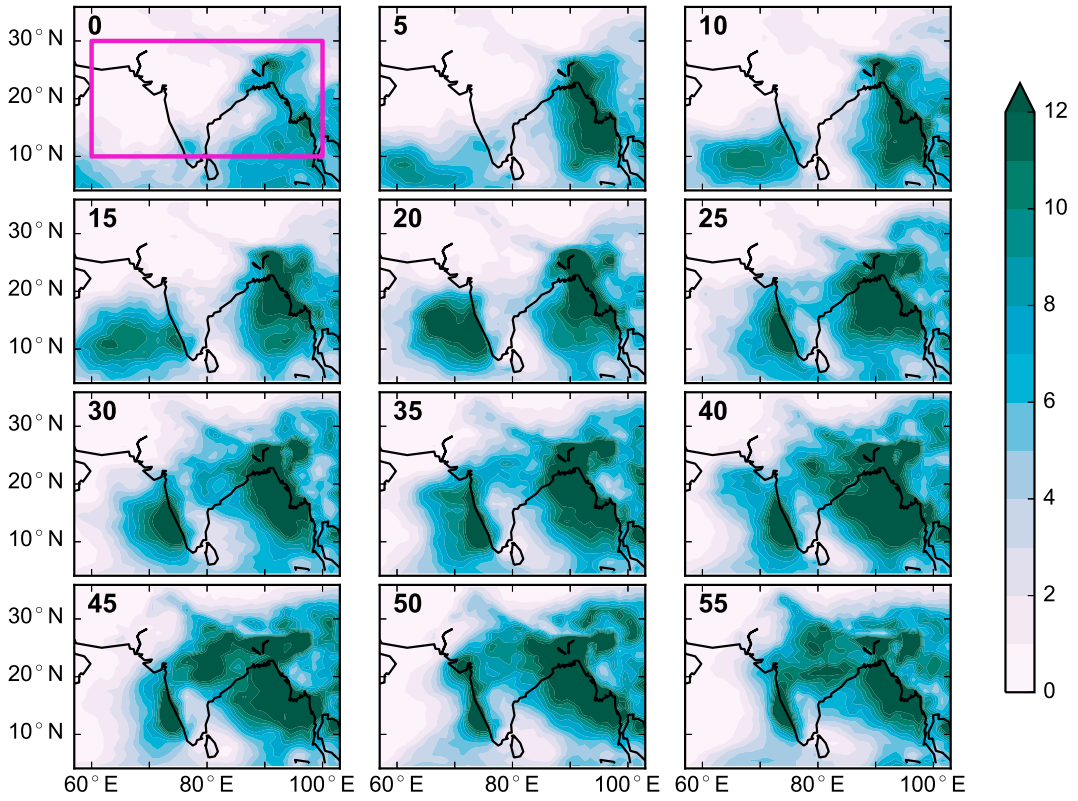

Figure 3. Maps of daily precipitation rates (mm d^{-1}) in GPCP climatological composites centered on onset date, for days 0 to 55. The magenta rectangle shows the averaging region for the CHP index.

points, we use GPCP cumulative precipitation, which is a smoother, nondecreasing function (since precipitation rates, unlike MFC, are nonnegative), and we average over a 4° × 4° area centered on each grid point, to smooth small-scale variability. We apply the change point detection method described in section 3.1 to define the local onset and withdrawal at each grid point.

Figure 4a shows the climatological mean and standard deviation of local onset dates, where regions with nonmonsoonal precipitation (June–September rainfall less than 50% of annual total, Figure S1) are masked out. We see a coherent region where the local onset dates are well defined, with standard deviations less than 20 days. In Kerala, local onset dates are very close to the climatological mean large-scale onset (day 138), although the southernmost region is masked because GPCP is unable to resolve all the regional features

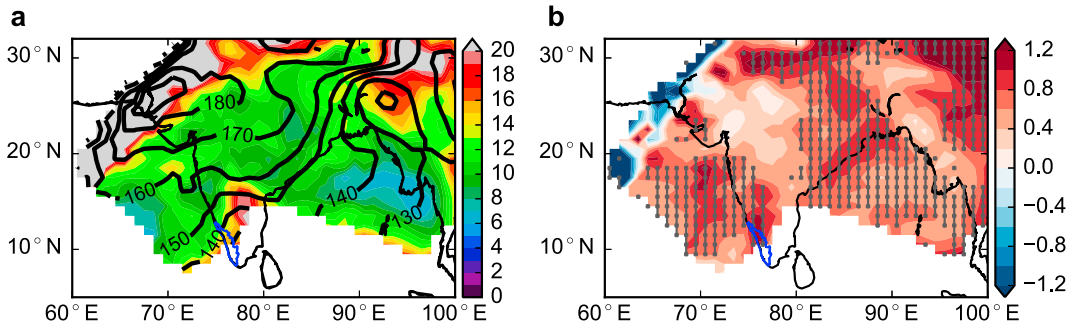

Figure 4. Local onset dates defined with CHP method using GPCP precipitation. (a) Climatological mean (contours) and standard deviation (colors) of onset dates. (b) Regression coefficients (d d^{-1}) of local onset dates onto large-scale CHP onset index, with gray stippling indicating the regions where the correlation is significant at the 5% level. Kerala state is outlined in blue.

(Figure S1). Going northward from Kerala, local onset dates are progressively later, with central and northeastern India having local onset dates up to 1 month after the large-scale onset.

Figure 4b shows the regression of local onset dates onto the large-scale onset date. Over the coherent region described for Figure 4a, the local onset dates are well correlated with the large-scale onset, with statistically significant regression coefficients of order 1 d d^{-1} over the peak rainfall regions. Thus, a later (earlier) large-scale onset corresponds to a delay (advance) of similar magnitude in local onset dates over the entire SASM region.

Toward the end of the season, the monsoon rain belts gradually withdraw southward across the region over approximately 1.5 months preceding the large-scale withdrawal date (Figures S6 and S7).

5. Conclusions

In this study, we have used the large-scale atmospheric moisture budget to propose a robust, objective definition of SASM onset and withdrawal, which captures the expected transitions in rainfall and winds. This method does not require any thresholds and is not susceptible to false onsets, making it ideal for analyzing variability and trends in SASM timing across data sets and climate models. CHP onset is highly correlated with the commonly used local operational index, the MOK, and is also correlated with subsequent variability of the SAMS: earlier onsets are associated with longer monsoon seasons and enhanced seasonal rainfall.

The use of change point detection allows us to precisely characterize the duration and abruptness of monsoon onset and to construct composites of the different stages of the monsoon that are characterized by different timescales. We show that CHP-based onset and withdrawal dates correspond with transitions in the large-scale SASM atmospheric moisture budget between negative and positive net precipitation. In the SASM sector mean, seasonal transitions in precipitation and circulation are strikingly similar to those in the zonal mean Hadley circulation, with a migration of the local ITCZ from the SH to the NH concurrent with a transition from an equinox regime with meridional overturning cells in each hemisphere to a solstice regime dominated by a single, cross-equatorial winter cell, and corresponding changes in upper level equatorial easterly jet and subtropical westerly jets.

Using the CHP method to define local onset and withdrawal dates at each grid point in the SASM domain, we find that local onset dates are approximately equal to the large-scale SASM onset date in Kerala and are progressively later further northward, with local onset dates up to 1 month after large-scale onset in central and northeastern India. The local onset dates are well correlated with the large-scale onset on interannual timescales, particularly in the peak rainfall regions, with a delay (advance) in large-scale onset associated with a delay (advance) of similar magnitude in local onset.

Future work includes using this newly defined index to quantify changes that occur in the leading energy and momentum budgets at SASM onset and withdrawal, as well as examining the reproducibility and future changes of SASM onset and withdrawal in models included in the CMIP5 archive.

Acknowledgments
This work was supported by the Caltech Terrestrial Hazard Observation and Reporting (THOR) Center. We thank Sabin TP for providing MOK data from the IMD. Reanalysis and precipitation data sources are cited in the text and referred to in the references list. MERRA-2 data are available at http://disc.sci.gsfc.nasa.gov/mdisc/. GPCP data are available at http://precip.gsfc.nasa.gov/. All other data and source code necessary to reproduce this analysis are available from the authors upon request (jwalker@caltech.edu).

References

Adamson, G. C. D., and D. J. Nash (2012), Long-term variability in the date of monsoon onset over western India, *Clim. Dyn.*, *40*, 2589–2603, doi:10.1007/s00382-012-1494-x.

Ananthakrishnan, R., and M. K. Soman (1988), The onset of the southwest monsoon over Kerala: 1901–1980, *J. Climatol.*, *8*(3), 283–296, doi:10.1002/joc.3370080305.

Boos, W. R., and K. A. Emanuel (2009), Annual intensification of the Somali jet in a quasi-equilibrium framework: Observational composites, *Q. J. R. Meteorol. Soc.*, *135*(639), 319–335, doi:10.1002/qj.388.

Bordoni, S., and T. Schneider (2008), Monsoons as eddy-mediated regime transitions of the tropical overturning circulation, *Nat. Geosci.*, *1*(8), 515–519, doi:10.1038/ngeo248.

Bosilovich, M., et al. (2015), MERRA-2: Initial Evaluation of the Climate, *NASA Tech. Rep. TM2015-104606, Ser. Glob. Model. Data Assim.*, 43, NASA. [Available at https://gmao.gsfc.nasa.gov/pubs/tm/docs/Bosilovich803.pdf.]

Cook, B. I., and B. M. Buckley (2009), Objective determination of monsoon season onset, withdrawal, and length, *J. Geophys. Res.*, *114*, D23109, doi:10.1029/2009JD012795.

Dima, I. M., and J. M. Wallace (2003), On the seasonality of the Hadley cell, *J. Atmos. Sci.*, *60*(12), 1522–1527, doi:10.1175/1520-0469(2003)060<1522:OTSOTH>2.0.CO;2.

Fasullo, J., and P. J. Webster (2003), A hydrological definition of Indian monsoon onset and withdrawal, *J. Clim.*, *16*(19), 3200–3211, doi:10.1175/1520-0442(2003)016<3200a:AHDOIM>2.0.CO;2.

Fieux, M., and H. Stommel (1977), Onset of the southwest monsoon over the Arabian Sea from marine reports of surface winds: Structure and variability, *Mon. Weather Rev.*, *105*(2), 231–236, doi:10.1175/1520-0493(1977)105<0231:OOTSMO>2.0.CO;2.

Flatau, M. K., P. J. Flatau, and D. Rudnick (2001), The dynamics of double monsoon onsets, *J. Clim.*, *14*(21), 4130–4146, doi:10.1175/1520-0442(2001)014<4130:TDODMO>2.0.CO;2.

Gadgil, S. (2003), The Indian monsoon and its variability, *Annu. Rev. Earth Planet. Sci.*, *31*(1), 429–467, doi:10.1146/annurev.earth.31.100901.141251.

Goswami, B. N. (2005), ENSO control on the south Asian monsoon through the length of the rainy season, *Geophys. Res. Lett.*, *32*, 2005–2007, doi:10.1029/2005GL023216.

Huang, B., V. F. Banzon, E. Freeman, J. Lawrimore, W. Liu, T. C. Peterson, T. M. Smith, P. W. Thorne, S. D. Woodruff, and H.-M. Zhang (2015), Extended Reconstructed Sea Surface Temperature Version 4 (ERSST.v4). Part I: Upgrades and Intercomparisons, *J. Clim.*, *28*(3), 911–930, doi:10.1175/JCLI-D-14-00006.1.

Huffman, G. J., D. T. Bolvin, and R. F. Adler (2016), GPCP Version 1.2 One-Degree Daily Precipitation Data Set, Research Data Archive at the National Center for Atmospheric Research, Computational and Information Systems Laboratory, Boulder, Colo., doi:10.5065/D6D50K46, Accessed 24 May 2016.

Huffman, G. J., R. F. Adler, M. M. Morrissey, D. T. Bolvin, S. Curtis, R. Joyce, B. McGavock, and J. Susskind (2001), Global precipitation at one-degree daily resolution from multisatellite observations, *J. Hydrometeorol.*, *2*(1), 36–50, doi:10.1175/1525-7541(2001)002<0036:GPAODD>2.0.CO;2.

Li, C., and M. Yanai (1996), The onset and interannual variability of the Asian summer monsoon in relation to land-sea thermal contrast, *J. Clim.*, *9*(2), 358–375, doi:10.1175/1520-0442(1996)009<0358:TOAIVO>2.0.CO;2.

Nguyen, H., A. Evans, C. Lucas, I. Smith, and B. Timbal (2013), The Hadley circulation in reanalyses: Climatology, variability, and change, *J. Clim.*, *26*(10), 3357–3376, doi:10.1175/JCLI-D-12-00224.1.

Noska, R., and V. Misra (2016), Characterizing the onset and demise of the Indian summer monsoon, *Geophys. Res. Lett.*, *43*, 4547–4554, doi:10.1002/2016GL068409.

Privé, N. C., and R. A. Plumb (2007), Monsoon dynamics with interactive forcing. Part I: Axisymmetric studies, *J. Atmos. Sci.*, *64*(5), 1417–1430, doi:10.1175/JAS3916.1.

Raju, P. V. S., U. C. Mohanty, and R. Bhatla (2007), Interannual variability of onset of the summer monsoon over India and its prediction, *Nat. Hazards*, *42*(2), 287–300, doi:10.1007/s11069-006-9089-7.

Ramage, C. (1971), Monsoon Meteorology, *Int. Geophys. Ser.*, vol. 15, 296 pp., Academic Press, San Diego, Calif.

Rao, Y. P. (1976), *South West Monsoon*, 376 pp., India Meteorological Department, Pune, India.

Rienecker, M. M., et al. (2011), MERRA: NASA's modern-Era retrospective analysis for research and applications, *J. Clim.*, *24*(14), 3624–3648, doi:10.1175/JCLI-D-11-00015.1.

Shaw, T. A. (2014), On the role of planetary-scale waves in the abrupt seasonal transition of the Northern Hemisphere general circulation, *J. Atmos. Sci.*, *71*(5), 1724–1746, doi:10.1175/JAS-D-13-0137.1.

Taniguchi, K., and T. Koike (2006), Comparison of definitions of Indian summer monsoon onset: Better representation of rapid transitions of atmospheric conditions, *Geophys. Res. Lett.*, *33*, L02709, doi:10.1029/2005GL024526.

Trenberth, K. E., J. Hurrell, and D. P. Stepaniak (2005), The Asian monsoon: Global perspectives, in *Asian Monsoon*, chap. 2, edited by B. Wang, pp. 67–87, Praxis Publ., Chichester, U. K.

Walker, J. M., S. Bordoni, and T. Schneider (2015), Interannual variability in the large-scale dynamics of the south Asian summer monsoon, *J. Clim.*, *28*(9), 3731–3750, doi:10.1175/JCLI-D-14-00612.1.

Wang, B., and LinHo (2002), Rainy season of the Asian-Pacific summer monsoon, *J. Clim.*, *15*(4), 386–398, doi:10.1175/1520-0442(2002)015<0386:RSOTAP>2.0.CO;2.

Wang, B., Q. Ding, and P. V. Joseph (2009), Objective definition of the Indian summer monsoon onset, *J. Clim.*, *22*(12), 3303–3316, doi:10.1175/2008JCLI2675.1.

Webster, P. J., and S. Yang (1992), Monsoon and ENSO: Selectively interactive systems, *Q. J. R. Meteorol. Soc.*, *118*(507), 877–926, doi:10.1002/qj.49711850705.

Weickmann, K. M., and R. M. Chervin (1988), The observed and simulated atmospheric seasonal cycle. Part I: Global wind field modes, *J. Clim.*, *1*(3), 265–289, doi:10.1175/1520-0442(1988)001<0265:TOASAS>2.0.CO;2.